Progress in Neurobiology 217 (2022) 102315

Contents lists available at ScienceDirect

Progress in Neurobiology

journal homepage: www.elsevier.com/locate/pneurobio

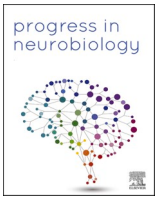

Macaque V1 responses to 2nd-order contrast-modulated stimuli and the possible subcortical and cortical contributions

Nian-Sheng Ju [a,1], Shu-Chen Guan [b,1], Shi-Ming Tang [a,b,c,*], Cong Yu [b,c,d,**]

[a] School of Life Sciences, Peking University, Beijing, China
[b] PKU-Tsinghua Center for Life Sciences, Peking University, Beijing, China
[c] IDG-McGovern Institute for Brain Research, Peking University, Beijing, China
[d] School of Psychological and Cognitive Sciences, Peking University, Beijing, China

ARTICLE INFO

Keywords:
Second-order stimuli
Orientation tuning
Primary visual cortex (V1)
Macaque
Two-photon imaging

ABSTRACT

Natural images comprise contours and boundaries defined by 1st-order luminance-modulated (LM) cues that are readily encoded by V1 neurons, and 2nd-order contrast-modulated (CM) cues that carry local, but not over-the-space, luminance changes. The neurophysiological foundations for CM processing remain unsolved. Here we used two-photon calcium imaging to demonstrate that V1 superficial-layer neurons respond to both LM and CM gratings in awake, fixating, macaques, with overall LM responses stronger than CM responses. Furthermore, adaptation experiments revealed that LM responses were similarly suppressed by LM and CM adaptation, with moderately larger effects by iso-orientation adaptation than by orthogonal adaptation, suggesting that LM and CM orientation responses likely share a strong orientation-non-selective subcortical origin. In contrast, CM responses were substantially more suppressed by iso-orientation than by orthogonal LM and CM adaptation, likely suggesting stronger orientation-specific intracortical influences for CM responses than for LM responses, besides shared orientation-non-selective subcortical influences. These results thus may indicate a subcortical-to-V1 filter-rectify-filter mechanism for CM processing: Local luminance changes in CM stimuli are initially encoded by orientation-non-selective subcortical neurons, and the outputs are half-wave rectified, and then summed by V1 neurons to signal CM orientation, which may be further substantially refined by intracortical influences.

1. Introduction

Contours and boundaries in natural images can be defined by 1st-order statistics, such as luminance, as well as by 2nd-order statistics, such as contrast. First-order luminance-modulated (LM) bars, edges, and gratings are readily processed by orientation-selective V1 neurons that are typically modeled as linear spatial filters (Hubel and Wiesel, 1959, 1962; Carandini et al., 1999). However, second-order contrast-modulated (CM) bars, edges, and gratings contain only local luminance changes, but no luminance changes over the space (See Fig. 2A for examples of LM and CM gratings). To explain CM stimulus processing, filter-rectify-filter (FRF) models (Fechner, 1860; Bergen and Adelson, 1988; Bergen and Landy, 1991; Graham and Sutter, 1998; Landy and Oruc, 2002) propose that linear filters first respond to local luminance changes (black and white dots in the CM grating of Fig. 2A), then their responses are nonlinearly rectified and summed by a larger second-stage linear filter. During nonlinear rectification, responses to dots at one polarity (e.g., black) are either nullified through half-wave rectification, or become equivalent to responses to dots at the other polarity (e.g., white) through full-wave rectification. The outputs are responses to dots at one single polarity (e.g., white), which are then summed by a second-stage filter.

The neuronal mechanisms underlying CM responses are not well understood. Single-unit recording studies revealed more A18/V2 neurons than A17/V1 neurons in cats and monkeys that respond to CM stimuli (Zhou and Baker, 1994; El-Shamayleh and Movshon, 2011; G. Li et al., 2014). In addition, there are reports that A17/V1 neurons may signal CM orientation through surround suppression when the inhibition

Abbreviations: CM, Contrast modulated; LM, Luminance modulated; SF, Spatial frequency; FOV, Field of view.

* Corresponding author at: School of Life Sciences, Peking University, Beijing, China.
** Corresponding author at: School of Psychological and Cognitive Sciences, Peking University, Beijing, China.
E-mail addresses: tangshm@pku.edu.cn (S.-M. Tang), yucong@pku.edu.cn (C. Yu).

[1] Equal contribution co-first authors.

https://doi.org/10.1016/j.pneurobio.2022.102315
Received 26 January 2022; Received in revised form 1 July 2022; Accepted 5 July 2022
Available online 7 July 2022

zones are elongated and orthogonal to a neuron's preferred orientation (H. Tanaka and Ohzawa, 2009; Hallum and Movshon, 2014), which would require sufficient aspect ratios of the orthogonal inhibition zones. In addition, Y cells in cat LGN can show cortical-cell-like CM responses at very high spatial frequencies (SFs) beyond neurons' first-order SF passbands as a result of response nonlinearity (Demb et al., 2001; Rosenberg et al., 2010), and Y-cell like neurons in cat A18 may receive direct inputs from LGN Y cells and respond to CM gratings (Gharat and Baker, 2017). This nonlinearity, however, cannot account for CM responses within the neurons' first-order SF passbands (El-Shamayleh and Movshon, 2011).

In this study, we used two-photon calcium imaging to compare the responses of macaque V1 neurons to LM and CM gratings. Two-photon imaging allows simultaneous recording of a large number of neurons, which would provide more comprehensive and less biased estimates of V1 neuronal responses to LM and CM stimuli, as well as respective orientation and SF tuning properties. Moreover, we used orientation adaptation to examine whether and how much LM and CM processing shares common mechanisms, and whether CM orientation processing, like LM orientation processing (Hubel and Wiesel, 1962; Tanaka, 1985; Reid and Alonso, 1995; Ferster et al., 1996), might receive subcortical contributions.

2. Materials and methods

2.1. Monkey preparation

Monkey preparations were identical to those reported in a previous study (Guan et al., 2021; Ju et al., 2021). Six rhesus monkeys (*Macaca mulatta*) aged 5–8 years were each prepared with two sequential surgeries under general anesthesia and strictly sterile condition. In the first surgery, a 20-mm diameter craniotomy was performed on the skull over V1. The dura was opened and multiple tracks of 100–150 nL AAV1.hSynap.GCaMP5G.WPRE.SV40 (AV-1-PV2478, titer 2.37e13 (GC/ml), Penn Vector Core) were pressure-injected at a depth of ~350 μm. Then the dura was sutured, the skull cap was re-attached with three titanium lugs and six screws, and the scalp was sewn up. After the surgery, the animal was returned to the cage, treated with injectable antibiotics (Ceftriaxone sodium, Youcare Pharmaceutical Group, China) for one week. Postop analgesia was also administered. The second surgery was performed 45 days later. A T-shaped steel frame was installed for head stabilization, and an optical window was inserted onto the cortical surface. Data collection could start as early as one week later. More details of the preparation and surgical procedures can be found in Li et al. (2017). The procedures were approved by the Institutional Animal Care and Use Committee, Peking University.

2.2. Behavioral task

After a ten-day recovery from the second surgery, monkeys were seated in primate chairs with head restraint. They were trained to hold fixation on a small white spot (0.1°) with eye positions monitored by an ISCAN ETL-200 infrared eye-tracking system (ISCAN Inc.) at a 120-Hz sampling rate. During the experiment, trials with the eye position deviated 1.5° or more from the fixation before stimulus offset were discarded as ones with saccades and repeated. For the remaining trials, the eye positions were mostly concentrated around the fixation point, with eye positions in over 95% of trials within 0.5° from the fixation. The viewing was binocular.

2.3. Visual stimuli

For Monkeys A, B, D, E, and F, visual stimuli were generated by the ViSaGe system (Cambridge Research Systems) and presented on a 21-

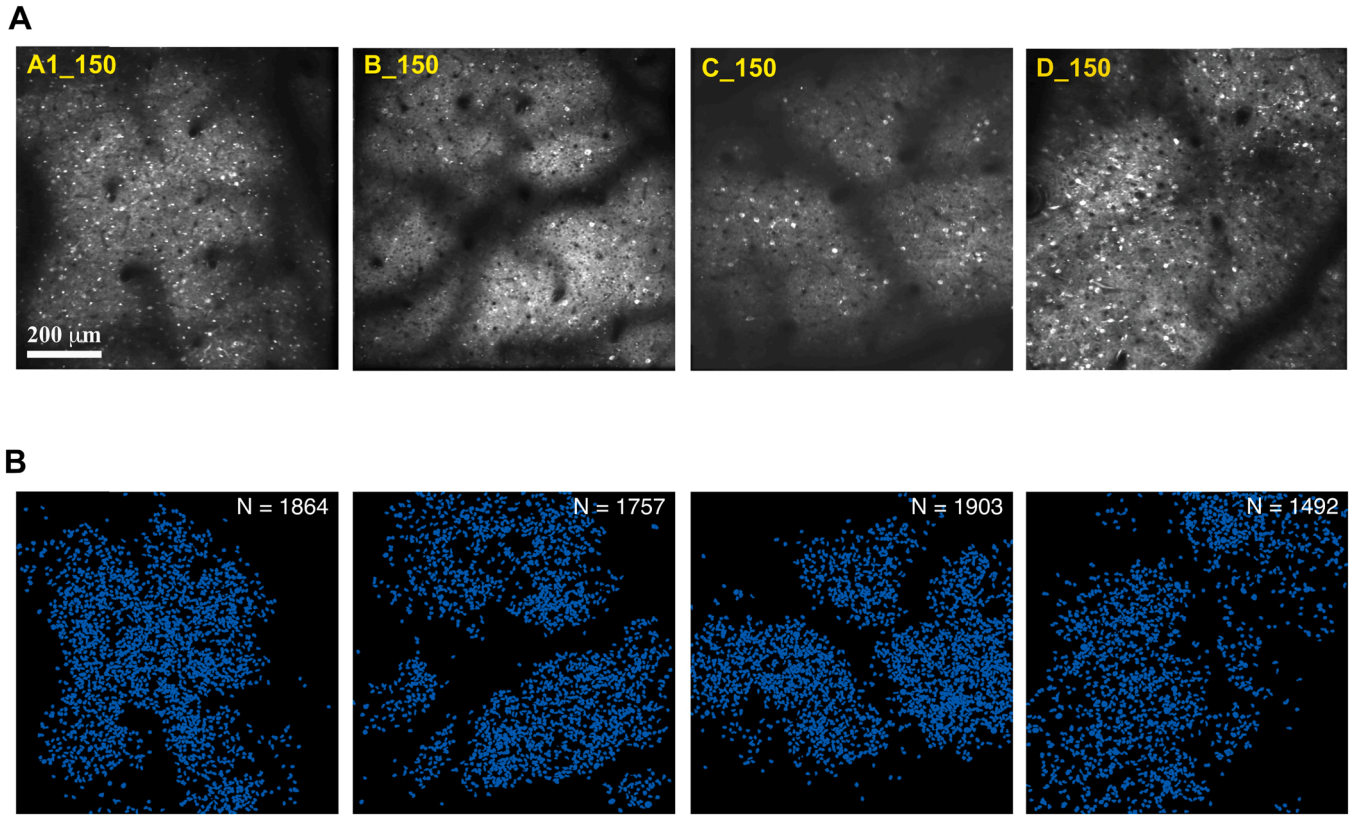

Fig. 1. Two-photon images. A. Examples of average two-photon images over a recording session. B. Extracted neurons highlighted with blue color from corresponding two-photon images.

inch Sony G520 CRT monitor (refresh rate = 80 Hz, resolution = 1280 pixel × 960 pixel, pixel size = 0.31 mm × 0.31 mm). Because of the space limit, the viewing distance varied depending on the stimulus spatial frequency (LM gratings: 30 cm at 0.25, 0.5, and 1 cpd, 60 cm at 2cpd, and 120 cm at 4 and 8 cpd; CM gratings: 30 cm at 0.25, 0.5, and 1 cpd, 60 cm at 2 and 4 cpd, and 120 cm at 8 cpd), except for Monkey F whose viewing distances were 45 cm at 0.25, 0.5, and 1 cpd and 180 cm at 2, 4, and 8 cpd (see Fig. 6). For Monkey C, visual stimuli were generated by Psychotoolbox 3 (Pelli and Zhang, 1991) and presented on a 27-inch Acer XB271HU LCD monitor (refresh rate = 80 Hz native, resolution = 2560 pixel × 1440 pixel native, pixel size = 0.23 mm × 0.23 mm). The viewing distance was 50 cm for lower

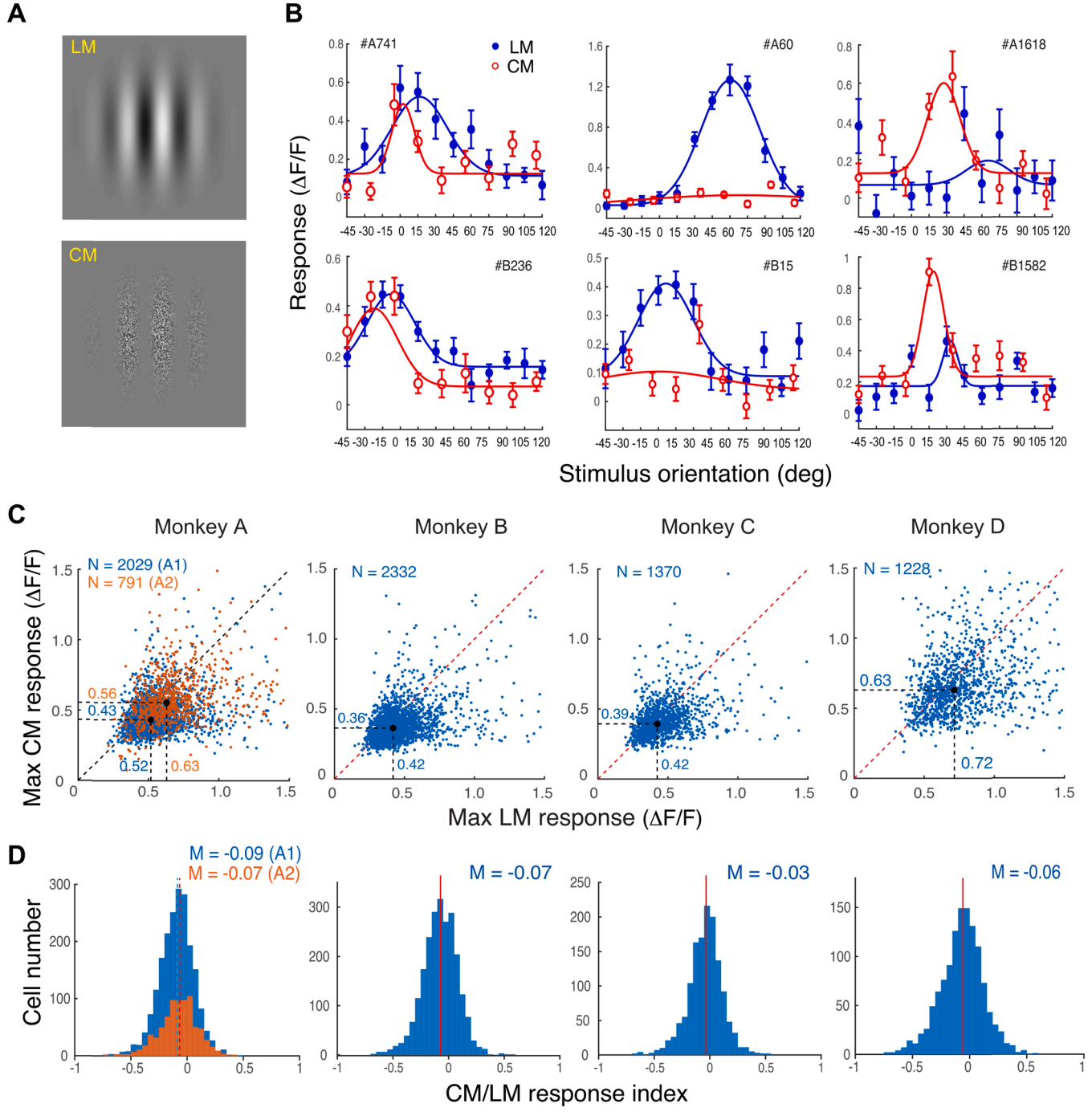

Fig. 2. Stimuli and comparisons of neuronal responses to LM and CM gratings. A. LM (top) and CM (bottom) gratings used in the experiments. The LM grating was a Gabor (a Gaussian-windowed sinusoidal grating). The CM grating was the same Gabor multiplied by binary noise. B. Responses of example neurons to LM and CM gratings at various orientations. The orientation tuning functions were fitted with a Gaussian function. Error bars indicate ± 1 SEM. C. Scatterplots of maximal CM vs. LM responses of neurons. Results at two recording depths of the same FOV in Monkeys A and B were pooled. Each dot represents one neuron's maximal CM and LM responses. The horizontal and vertical dashed lines indicate medians. See Fig. S1A for similar results when all orientation neurons before Gaussian fitting are considered. D. Distributions of CM-LM response indices (CLIs). A neuron would prefer a LM grating more if CLI < 0. The vertical lines indicate medians. M: Median. See Fig. S1B for similar results when all orientation neurons before Gaussian fitting are considered. Note: The LM data of current Monkeys A and B were from the same data sets of Monkeys C and D in two earlier papers (Guan et al., 2021; Ju et al., 2021), and were reanalyzed in this study for comparisons with CM data collected during the same period.

frequencies (0.25–2 cpd) and 100 cm for higher frequencies (4 & 8 cpd). For both monitors, the screen luminance was linearized by an 8-bit look-up table, and the mean luminance was ~47 cd/m^2.

A drifting square-wave grating (SF = 4 cpd, contrast = full, speed = 3 cycles/s, starting phase = 0°, and size = 0.4° in diameter) was first used to determine the location, eccentricity (typically 2–5°) and size (typically 0.8 – 1°) of the population receptive field associated with a recording field of view (FOV), as well as ocular dominance columns when monocularly presented to confirm the V1 location. This fast process used a 4 × objective lens mounted on the two-photon microscope and revealed no cell-specific information.

Four monkeys (Monkeys A-D) participated in the first experiment that compared neuronal responses to LM and CM stimuli (Fig. 2A). Cell-specific responses were measured with a high-contrast (0.9) LM stimulus, which was a Gabor grating (Gaussian-windowed sinusoidal grating) drifting at 2 cycles/s in opposite directions perpendicular to the Gabor orientation, or a CM stimulus, which was the same Gabor grating multiplied by binary noise of 1 or − 1. The binary noise was regenerated every frame. The starting phase of the drifting Gabors was always 0°. The Gabor grating varied at 12 orientations from 0° to 165° in 15°-steps, and 6 SFs from 0.25 to 8 cpd in 1-octave steps. In addition, three stimulus sizes (with constant stimulus centers) were used at each SF for two purposes. First, our pilot measurements suggested very strong surround suppression with large stimuli. Therefore, comparing the responses to different stimulus sizes helped approximate the RF size of each neuron that produced the maximal response and least surround suppression. Second, for neurons whose RF centers and the stimulus center were misaligned, the RFs of some misaligned neurons might be better covered by larger stimuli. Still, for neurons whose RFs were partially overlapping with the stimuli, their responses would be weaker and not much orientation-selective because the Gaussian-blurred low-contrast stimulus edge contained little orientation information. Therefore, these neurons would most likely be filtered out during our multiple steps of selection of orientation-tuned neurons (see below). Specifically, the σ of the Gaussian envelope of the Gabor was 0.64λ and 0.85λ at all SFs, and was additionally smaller at 0.42λ when SFs were 0.25–1 cpd, and larger at 1.06λ when SFs were 2–8 cpd (λ: wavelength; Gabors with the same σ in wavelength unit had the same number of cycles). Here at the smallest σ (0.42λ), the Gabors still had sufficient number of cycles (frequency bandwidths = 1 octave) (Graham, 1989), so that the actual stimulus SFs were precise at nominal values. In terms of visual angle, σ = 1.68°, 2.56°, and 3.36° at 0.25 cpd; 0.84°, 1.28°, and 1.68° at 0.5 cpd; 0.42°, 0.64°, and 0.85° at 1 cpd; 0.34°, 0.42°, and 0.53° at 2 cpd; 0.17°, 0.21°, and 0.26° at 4 cpd, and 0.08°, 0.11°, and 0.13° at 8 cpd, respectively. For CM Gabors, the visual angle size of the noise element was constant at 3.57 x 3.57 arcmin^2 when the CRT monitor was used, and 1.58 x 1.58 arcmin^2 when the LCD monitor was used (the physical size changed at different viewing distances).

Each stimulus was presented for 1000 ms, with an inter-stimulus interval (ISI) of 1500 ms that was sufficient to allow the calcium signals back to the baseline level (Guan et al., 2020). Each stimulus condition was repeated 12 times with six repeats for each opposite direction. Imaging of neuronal responses to either LM or CM stimuli at a specific FOV and depth (e.g., LM stimuli/Monkey A1/150 μm), including all orientation, SF, and size conditions, was completed in one session that lasted 3–4 h. During the session, recording at a specific viewing distance was completed before moving to the next one, with all stimuli in each distance pseudo-randomly presented.

2.4. Two-photon imaging

Two-photon imaging was performed with a Prairie Ultima IV (In Vivo) two-photon microscope (Prairie Technologies) (all monkeys except C) or a FENTOSmart two-photon microscope (Femtonics) (Monkey C), and a Ti:sapphire laser (Mai Tai eHP, Spectra Physics). One or two FOVs of 850 × 850 μm^2 were selected in each animal and imaged under a 16 × objective lens (0.8 N.A., Nikon) at a resolution of 1.6 μm/pixel, with the use of 1000-nm femtosecond laser. Fast resonant scanning mode (32 fps) was chosen to obtain continuous images of neuronal activity (8 fps after averaging every 4 frames). For either LM or CM stimuli, recordings at two depths of the same FOV were completed in two consecutive days. For Monkeys A-C, recording was first performed at 150 μm with LM stimuli. Some neurons with high brightness or unique dendrite patterns were selected as landmarks. In the next LM session and later CM sessions, the same FOV at 150 μm was located before recording with the help of landmarks, and the depth plane was lowered if recording was performed at 300 μm. CM recordings were performed 1–5 days after LM recordings. For Monkey D, the order of LM and CM testing was reversed. Because of the time limit, the same stimuli at two depths, or LM and CM stimuli at the same depth, could not be completed in a single session, but the same neurons could be precisely tracked over multiple recording sessions with the use of multiple landmark cues.

2.5. Imaging data analysis: Initial screening of ROIs

Data were analyzed with customized MATLAB codes. A normalized cross-correlation based translation algorithm was used to reduce motion artifacts (M. Li et al., 2017). Then fluorescence changes were associated with corresponding visual stimuli through the time sequence information recorded by Neural Signal Processor (Cerebus system, Blackrock Microsystem). By subtracting the mean of the 4 frames before stimuli onset (*F0*) from the average of the 6th-9th frames after stimuli onset (*F*) across 5 or 6 repeated trials for the same stimulus condition (same orientation, spatial frequency, size, and drifting direction), the differential image ($\Delta F = F - F0$) was obtained.

The regions of interest (ROIs) or possible cell bodies were decided through sequential analysis of 432 differential images in the order of stimuli type (2), SF (6), size (3), and orientation (12) (2 ×6×3 ×12 = 432). The first differential image was filtered with a band-pass Gaussian filter (size = 2–10 pixels), and connected subsets of pixels (>25 pixels, which would exclude smaller vertical neuropils) with average pixel value > 3 standard deviations of the mean brightness were selected as ROIs. Then the areas of these ROIs were set to mean brightness in the next differential image before the bandpass filtering and thresholding were performed (This measure gradually reduced the SDs of differential images and facilitated detection of neurons with lower fluorescence responses). If a new ROI and an existing ROI from the previous differential image overlapped, the new ROI would be on its own if the overlapping area OA < 1/4 ROI$_{new}$, discarded if 1/4 ROI$_{new}$ < OA < 3/4 ROI$_{new}$, and merged with the existing ROI if OA > 3/4 ROI$_{new}$. The merges would help smooth the contours of the final ROIs. This process went on through all differential images twice to select ROIs. Finally, the roundness for each ROI was calculated as:

$$Roundness = \frac{\sqrt{4\pi \times A}}{P}$$

where *A* was the ROI's area, and *P* was the perimeter. Only ROIs with roundness larger than 0.9, which would exclude horizontal neuropils, were selected (Fig. 1B).

2.6. Imaging data analysis: Orientation-/SF-tuned neurons

The ratio of fluorescence change ($\Delta F/F0$) was calculated as a neuron's response to a specific stimulus condition. For a specific neuron's response to a specific stimulus condition, the $F0_n$ of the n-th trial was the average of 4 frames before stimulus onset, and F_n was the average of 5th-8th or 6th-9th frames after stimulus onset, whichever was greater. $F0_n$ was then averaged across 12 trials to obtain the baseline F0 for all trials (for the purpose of reducing noises in the calculations of responses), and $\Delta F_n/F0 = (F_n\text{-}F0)/F0$ was taken as the neuron's response to this

stimulus with this trial. For a small portion of neurons (e.g., ~3% in Monkeys A and B when responding to LM Gabors) showing direction selectivity as their responses to two opposite directions differed significantly ($p < 0.05$, Friedman test), the 6 trials at the preferred direction was considered for calculations of $\Delta F_n/F0$ as the cell's responses to a particular stimulus. F0 was still averaged over 12 trials at two opposite directions.

Several steps were then taken to decide whether a neuron was tuned to orientation and/or spatial frequency of LM or CM stimuli. First, the orientation, SF, and size (σ) producing the maximal response among all LM or CM conditions were selected. Then responses to other 11 orientations were decided at the selected SF, and 5 SFs were decided at the selected orientation, all at the same selected size. Second, to select orientation and/or SF tuned neurons, a non-parametric Friedman test was performed to test whether a neuron's responses at 12 orientations or 6 SFs were significantly different from each other. To reduce Type-I errors, the significance level was set at $\alpha = 0.01$. Third, for those showing significant orientation difference, the trial-based orientation responses of each neuron were fitted with a Gaussian model:

$$R(\theta) = a_1 2^{-\left(\frac{\theta-\theta_0}{\sigma}\right)^2} + b$$

where R(θ) was the response at orientation θ, and free parameters a_1, θ_0, σ, and b were the amplitude, peak orientation, standard deviation of the Gaussian function, and minimal response of the neuron, respectively. Only neurons with the coefficient of determination $R^2 > 0.5$ for at least one type of stimuli (LM/CM) were finally selected for data analysis unless otherwise stated. The amplitude parameter a1 was positive in all selected orientation neurons. Fourth, for those showing significant SF difference, the trial-based SF responses of each neuron were fitted with a Difference-of-Gaussian model.

$$R(sf) = a_1 e^{-\left(\frac{sf}{\sigma_1}\right)^2} - a_2 e^{-\left(\frac{sf}{\sigma_2}\right)^2} + b$$

where R(sf) was a neuron's response at spatial frequency sf, free parameters a_1, σ_1, a_2, and σ_2 were amplitudes and standard deviations of two Gaussians, respectively, and b was the minimal response among 6 spatial frequencies. Only those with $R^2 > 0.5$ were included for data analysis.

2.7. Adaptation experiment

Monkeys C, D, and a new Monkey E participated in the adaptation experiment (Figs. 4 & 5). Pre-adaptation neuronal responses to LM and CM Gabor gratings (Fig. 2A) at 6 (Monkey C) or 12 (Monkeys D & E) equally spaced orientations (contrast = 0.9) were first recorded. The stimulus SF was set at 3 cpd for Monkeys C & E and 4 cpd for Monkey D, which were near the median preferred SFs with CM gratings of Monkeys C (2.9 cpd) and D (4.1 cpd), respectively, in the earlier experiment (Fig. S2). Monkey E did not participate in the earlier experiment, so we took 3 cpd from Monkey C because two monkeys were recorded at similar eccentricities (1.88° and 2.06° for Monkey C and E, respectively). Only one stimulus size was used ($\sigma = 0.85\lambda$, or 0.28° at 3 cpd and 0.21° at 4 cpd). Because the central area of a Gabor stimulus up to a radius of around 2σ has sufficient contrast energy, the effect stimulus size here would be approximately 1.12° at 3 cpd and 0.84° at 4 cpd, similar to the population RF of 0.8–1°. This pre-adaptation procedure identified orientation-selective LM and CM neurons activated with the current stimuli and obtained each neuron's preferred LM and CM orientations, respectively, as pre-adaptation baselines.

Then the monkeys were adapted to a LM or CM adaptor, and the adaptation effects were measured with LM and CM testing stimuli at respective LM and CM preferred and orthogonal orientations, with stimuli identical to those used in pre-adaptation measurements. An adaptation stimulus sequence included 20 repeats of $AAT_{n1}AAT_{n2}AAT_{n3}AAT_{n4}$, where A was the LM or CM adaptor at one of six equally spaced adaptor orientations, and the test stimuli $T_{n1\text{-}n4}$ were LM and CM gratings whose orientations were either the same as, or orthogonal to, the adaptor orientation, and were presented in a random order (illustrated in Figs. 4A & 5A). Because each stimulus was presented for 1 s with a 1.5-s inter-stimulus interval, a specific test stimulus (e.g., T_{n4}) in an adaptation stimulus sequence was repeated every 30 s (12 conditions x 2.5 s) on average or longer (counting monkey's re-fixating time when the fixation was off), which minimized self-adaptation. The post-adaptation response to a specific test stimulus was the averaged responses of 20 repeats.

3. Results

We first recorded responses of V1 superficial-layer neurons to drifting LM and CM Gabor gratings (Fig. 2A) in four awake, fixating macaque monkeys. Monkey A had two recording fields of view (FOVs), and Monkeys B-D each had one FOV. Imaging was performed at two cortical depths (150 and 300 μm from the cortical surface) for Monkeys A and B, and at one depth for Monkeys C and D (150 μm). Imaging processing and data analysis identified 4972, 3370, 1903, and 1492 neurons in Monkeys A-D, respectively. Among them, 4247 (85.4%), 3085 (91.5%), 1757 (92.3%), and 1398 (93.7%) neurons showed orientation tuning with LM and/or CM stimuli (Friedman test). Gaussian fitting (Fig. 2B) further selected 2820 (56.7%), 2332 (69.2%), 1370 (72.0%), and 1228 (82.3%) neurons for data analysis unless otherwise stated.

Example neurons show that some neurons preferred both LM and CM gratings (Fig. 2B, left column), some mainly preferred LM gratings (middle column), and some mainly preferred CM gratings (right column). When the maximal LM and CM responses of each neuron estimated with Gaussian fitting were contrasted (Fig. 2C), the medians of maximal LM responses were higher than those of maximal CM response, by 18.6% in Monkey A, 16.7% in Monkey B, 7.7% in Monkey C, and 14.3% in Monkey D (Data were similar at two depths of the same FOV in Monkeys A and B, and were thus pooled here and later). A CM-LM response index (CLI) was calculated for each neuron: $CLI = (R_{max\_CM} - R_{max\_LM}) / (R_{max\_CM} + R_{max\_LM})$, so that $CLI < 0$ would indicate more LM preference, and $CLI > 0$ would indicate more CM preference. Fig. 2D shows unimodal CLI distributions in all monkeys, with CLI medians biased toward a preference for LM stimuli. Overall, 67.4% of neurons (weighted average) preferred LM to CM stimuli (CLI indices < 0). The results were similar if all orientation-tuned neurons before Gaussian fitting were considered (Fig. S1).

3.1. Neuronal orientation tuning with LM and CM stimuli

Based on Gaussian fitting of orientation responses, we divided the same sets of neurons in Fig. 2D into three categories: LM_{ORI_only} neurons which were only tuned to LM grating orientation (only the coefficient of determination $R^2_{LM} > 0.5$), CM_{ORI_only} neurons which were only tuned to CM grating orientation (only $R^2_{CM} > 0.5$), and LM_{ORI}+CM_{ORI} neurons which were tuned to both LM and CM grating orientations ($R^2_{LM} > 0.5$ & $R^2_{CM} > 0.5$). Fig. 3A indicates that more than half of the neurons were LM_{ORI_only} neurons, roughly 20–30% were LM_{ORI}+CM_{ORI} neurons, and 10–20% were CM_{ORI_only} neurons.

The LM orientation maps, which contained LM_{ORI_only} and LM_{ORI}+CM_{ORI} neurons, showed clustering of neurons tuned to similar orientations (Fig. 3B upper). However, orientation clustering in CM (CM_{ORI_only} and LM_{ORI}+CM_{ORI}) maps (Fig. 3B lower) was less clear, partly because of fewer CM_{ORI_only} neurons, except in C_150, which contained more CM_{ORI_only} neurons and showed similar orientation clustering to that in the corresponding LM map.

Previous studies have revealed that LM_{ORI}+CM_{ORI} neurons may not necessarily have the same LM and CM orientation preferences (El-Shamayleh and Movshon, 2011). The frequency distributions of preferred LM and CM orientations were plotted for LM_{ORI}+CM_{ORI} neurons in each

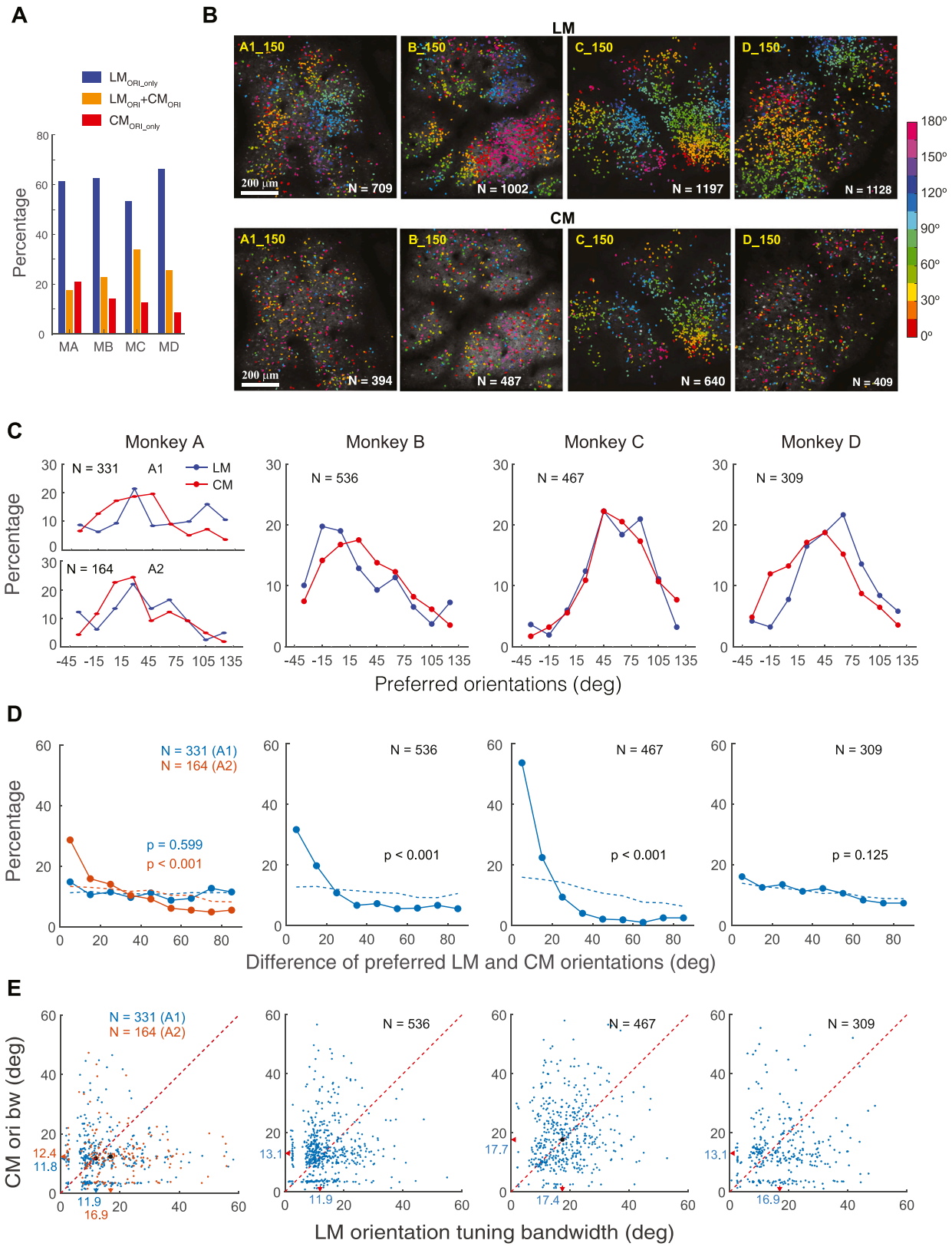

Fig. 3. Orientation tuning of V1 neurons to LM and CM gratings. A. Percentage distributions of LM_{ORI_only}, CM_{ORI_only}, and LM_{ORI}+CM_{ORI} neurons on the basis of Gaussian fitting in four monkeys. B. Examples of functional maps of LM orientation tuning by LM_{ORI_only} and LM_{ORI}+CM_{ORI} neurons (upper panels), and CM orientation tuning by CM_{ORI_only} and LM_{ORI}+CM_{ORI} neurons (lower panels). C. Frequency distributions of preferred LM and CM orientations by LM_{ORI}+CM_{ORI} neurons. D. Frequency distributions of neurons against the difference of preferred LM and CM orientations by LM_{ORI}+CM_{ORI} neurons. The dashed lines are simulated baselines indicating null distributions of differences in randomly paired LM and CM orientation preferences across neurons. E. The LM vs. CM orientation tuning bandwidths (half height at half width) of each LM_{ORI}+CM_{ORI} neuron. Arrows indicate medians. Note: Summary statistics of neurons' SF tuning with LM and CM stimuli are presented in Figs. S2B & S2C.

monkey in Fig. 3C. The orientation bias shown in each FOV was consistent with our previous report that the orientation distributions (of LM neurons) vary substantially within and among individual FOVs, which are minimized when data from multiple FOVs are pooled (Ju et al., 2021). The corresponding frequency distributions of orientation preference differences were plotted in Fig. 3D. Neurons in Monkeys A (FOV 1) and D tended to have mostly unrelated LM and CM orientation preferences, which were not significantly different from random ($p = 0.60$ and 0.13, respectively, permutation test) (Fig. 3D). In contrast, those in Monkeys A (FOV 2), B, and C more likely preferred similar LM and CM orientations (higher frequencies at small tuning differences) rather than random (all $p < 0.001$, permutation test) (Fig. 3D). The large variations thus appeared to be contingent on specific FOVs, but not monkeys. However, the median LM and CM orientation bandwidths (half width at half height) were similar, differing by less than 4° in all animals, although the variations among neurons were quite large (Fig. 3E). The LM and CM orientation bandwidths also differed by less than 4° when all LM (LM_{ORI_only} and $LM_{ORI}+CM_{ORI}$) and all CM (CM_{ORI_only} and $LM_{ORI}+CM_{ORI}$) neurons in Fig. 3A were considered (Fig. S2A).

3.2. Orientation adaptation effects

Next, we ran an orientation adaptation experiment on Monkeys C, D, and E to explore the possible neural mechanisms of CM processing and the relationship between neuronal LM and CM responses in V1. Two conjectures were made. First, if V1 orientation responses to LM and CM gratings share some cortical mechanisms, the peak response of a specific neuron to one type of stimulus would be at least partially suppressed by adapting to the other type of stimulus at the same orientation. Second, if V1 neuronal responses to CM patterns, like to LM patterns, also have a subcortical origin (Hubel and Wiesel, 1962; K. Tanaka, 1985; Reid and Alonso, 1995; Ferster et al., 1996), or more specifically, if V1 receptive fields take in half-wave rectified responses of subcortical neurons to individual black and white dots, then the peak response of a specific neuron to one type of stimulus would be at least partially suppressed by adapting to either the same or the other type of stimulus at an orthogonal orientation. This is because subcortical neurons have little orientation selectivity, and there is evidence that the responses of LGN cells can be at least partially suppressed by adaptation at any orientation (Solomon et al., 2004; Camp et al., 2009). This subcortical-to-V1 filter-rectify-filter process also applies to the formation of LM orientation since ON and OFF LGN responses were separately summed according to Hubel and Wiesel (1962).

3.2.1. Adaptation effects on LM responses

We found that the responses of LM neurons (including both LM_{ORI_only} and $LM_{ORI}+CM_{ORI}$ neurons) to a LM grating at the preferred orientation were reduced not only by iso-oriented LM adaptors, but also by iso-oriented CM adaptors (Fig. 4). Moreover, peak LM responses were also moderately more suppressed by iso-oriented LM and CM adaptors than by orthogonal LM and CM adaptors. Although not consistently appreciable in four example neurons' pre-adaptation orientation tuning functions and post-adaptation responses (Fig. 4B), these trends were evident in median pre- vs. post-adaptation responses of neurons at preferred orientations (Fig. 4C). We used an adaptation effect index (AEI) to characterize the response changes before and after adaptation. $AEI = (R_{pre} - R_{post})/(R_{pre} - R_{ortho})$, where R_{pre} and R_{ortho} were pre-adaptation responses to the LM (here) or CM (later) test stimuli at the preferred and orthogonal orientations, and R_{post} was the post-adaptation response to the LM or CM test stimuli at the preferred orientation. $AEI = 0$ would indicate no adaptation effect (no reduction of neural response), and $AEI = 1$ would indicate that the peak response at the preferred orientation was reduced to the pre-adaptation response level at an orthogonal orientation. Fig. 4D shows AEIs (median ± 25 percentiles) of LM responses by different types of adaptors for each monkey, which were analyzed with a mixed-design ANOVA with Adaptor-type (LM vs. CM) and Adaptor-orientation (iso vs. ortho) as within-subject factors and Animal (Monkeys C-E) as a between-subject factor. The ANOVA outcomes indicated that AEIs were not significantly affected by Adaptor-type ($F_{1, 679} = 2.12$, $p = 0.146$), but by Adaptor-orientation ($F_{1, 679} = 39.12$, $p < 0.001$) with a moderate effect size (partial $\eta^2 = 0.054$, close to 0.06 for a medium effect size) and Animal ($F_{2, 679} = 7.67$, $p < 0.001$) with a small effect size (partial $\eta^2 = 0.022$). There were significant interactions between Animal and Adaptor-type ($F_{2, 679} = 5.90$, $p = 0.003$, partial $\eta^2 = 0.017$) and between Animal and Adaptor-orientation ($F_{2, 679} = 10.04$, $p < 0.001$, partial $\eta^2 = 0.029$). The significant main effect of Animal and its interactions with Adaptor-type and Adaptor-orientation suggest inter-animal differences in these measures.

3.2.2. Adaptation effects on CM responses

The responses of CM neurons (including both CM_{ORI_only} and $LM_{ORI}+CM_{ORI}$ neurons) to a CM grating at the preferred orientation were suppressed by adaptation to iso-oriented LM and CM adaptors. They were also substantially more suppressed by iso-oriented LM and CM adaptors than by orthogonal LM and CM adaptors (Fig. 5). Fig. 5B presents four example CM neurons' pre-adaptation orientation tuning functions and post-adaptation responses with four types of adaptors. Fig. 5C contrasts all individual CM neurons' pre- and post-adaptation responses at the preferred orientation, as well as their medians. Fig. 5D shows AEIs of CM responses by different types of adaptors for each monkey, which were again analyzed with a mixed-design ANOVA with Adaptor-type (LM vs. CM) and Adaptor-orientation (iso vs. ortho) as within-subject factors and Animal (Monkeys C-E) as a between-subject factor. The ANOVA outcomes indicated that AEIs were significantly affected by Adaptor-type ($F_{1, 362} = 18.74$, $p < 0.001$) but with a relatively small effect size (partial $\eta^2 = 0.049 < 0.06$ for a medium effect size). However, AEIs were also significantly affected by Adaptor-orientation ($F_{1, 362} = 64.92$, $p < 0.001$) with a large effect size (partial $\eta^2 = 0.152 > 0.14$ for a large effect size, larger than corresponding partial $\eta^2 = 0.054$ with LM responses in Fig. 4), confirming that LM and CM responses were more suppressed by iso-oriented LM and CM adaptors than by orthogonal ones, and the orientation difference was more evident with peak CM responses here than with peak LM responses in Fig. 4. In addition, there were also a significant main effect of Animal ($F_{2, 362} = 5.18$, $p = 0.006$, partial $\eta^2 = 0.028$) and significant interactions between Animal and Adaptor-type ($F_{2, 362} = 3.79$, $p = 0.023$, partial $\eta^2 = 0.021$) and between Animal and Adaptor-orientation ($F_{2, 362} = 5.07$, $p = 0.003$, partial $\eta^2 = 0.031$), indicating inter-animal differences in these measures.

Overall the results were consistent with our two conjectures. First, LM and CM responses at respective preferred orientations were suppressed by the other type of adaptors at the iso orientation (isoCM and isoLM adaptors, respectively), consistent with the first conjecture that V1 responses to LM and CM gratings share certain cortical mechanisms. Second, LM and CM responses at respective preferred orientations were more or less suppressed by orthogonal LM or CM adaptation, consistent with the second conjecture that CM responses, like LM responses, may also have a subcortical origin (more in Discussion).

3.3. Control: The possible role of screen luminance nonlinearity in CM responses

One longstanding issue with CM stimuli is that monitor gamma correction may not compensate screen luminance nonlinearity completely, which would generate low-contrast luminance cues in CM stimuli, so that the responses of LM neurons to these cues may be mistakenly interpreted as CM responses (Zhou and Baker, 1994). In a control experiment with a new Monkey F, we compared LM and CM responses at different SFs while deliberately making the binary noises invisible at half the SFs. The stimulus sizes (σ) at each SF were the same as those in the first experiment (Fig. 2), but the size of binary noise

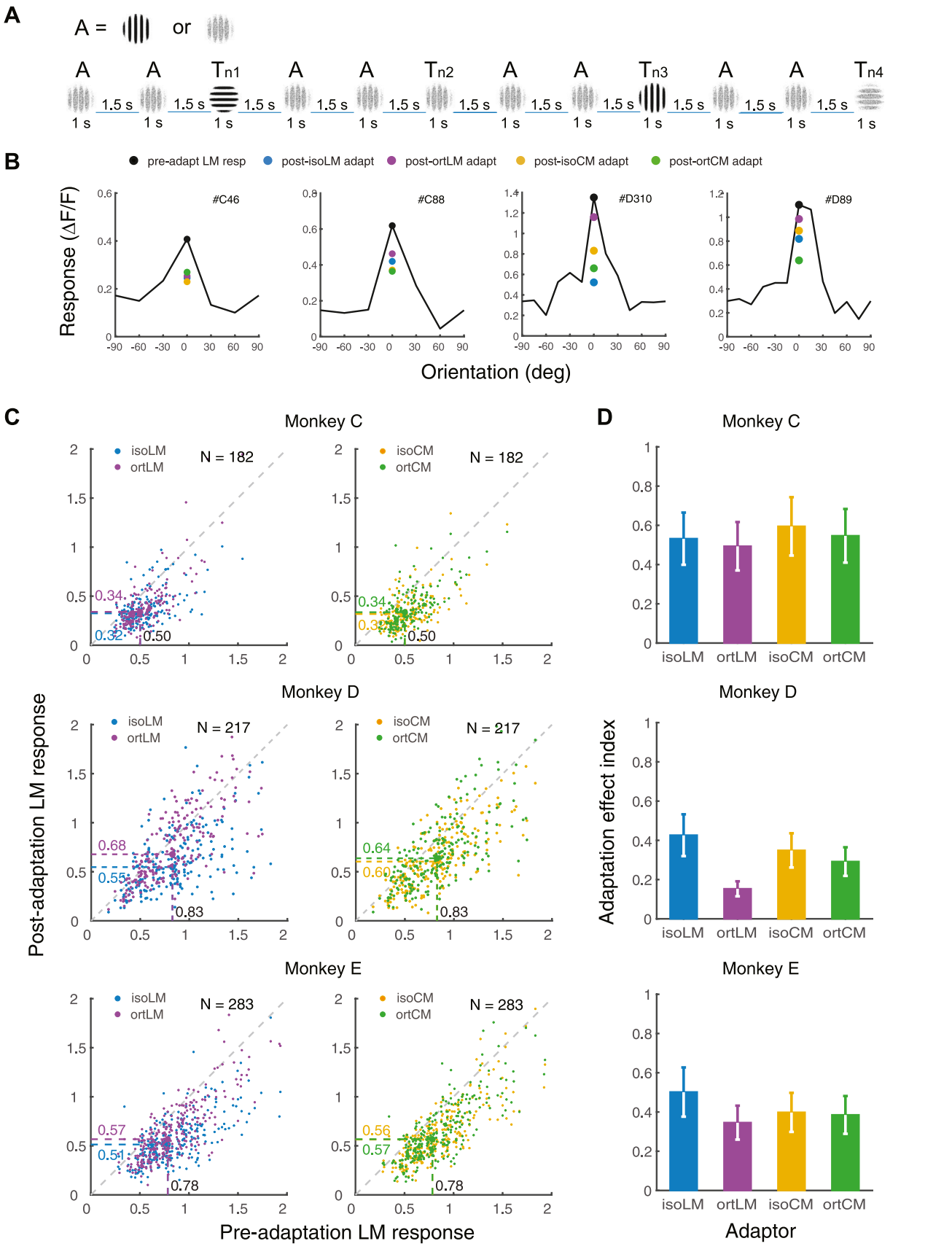

(caption on next page)

Fig. 4. The effects of adaptation on V1 neuronal responses to LM gratings. A. Illustration of an adaptation stimulus sequence $AAT_{n1}AAT_{n2}AAT_{n3}AAT_{n4}$. A was a CM (shown in the sequence) or LM adaptor at one of six orientations. $T_{n1\text{-}n4}$ were the LM and CM gratings whose orientations were either the same as, or orthogonal to, the adaptor orientation, and were presented in a random order. The inter-stimulus interval could be longer than 1.5 s when refixation was necessary. B. The orientation tuning function of four example neurons with LM gratings and the responses at the peak orientation after adaptation to four types of adaptors, respectively. C. Scatterplots of individual neurons' LM responses at the peak orientation before and after adaptation. The dashed lines indicate median responses. Data points below the diagonal line indicate suppressed responses after adaptation. Left panels: Results with LM adaptors. Right panels: Results with CM adaptors. D. The adaptation effect indices for LM responses with 4 types of adaptors. Similar results were obtained when AEI data with LM_{ORI_only} neurons and LM_{ORI}+CM_{ORI} neurons were analyzed separately (Fig. S3A). Error bars indicate 25 and 75 percentiles.

elements was fixed at 1 × 1 pixel. For SFs at 0.25, 0.5, and 1 cpd, the viewing distance was set at 0.45 m, so that each individual pixel was 2.36 arcmin in size, equal to a maximal and still visible SF of 12.7 cpd (the actual SFs in local areas could be lower when more than one pixel of the same polarity was connected). However, for SFs at 2, 4, and 8 cpd, the viewing distance was quadrupled to 1.80 m, so that each individual pixel size was 0.59 arcmin , equivalent to a maximal SF of up to 50.8 cpd, which was below the parafoveal spatial resolution limit and thus invisible. What is left with these higher-SF stimuli would be potential low-contrast luminance cues. Therefore, recorded responses at these SFs, if present, would reflect remaining display luminance nonlinearity.

The SF tuning functions of 3 example LM_{ORI}+CM_{ORI} neurons and the average population responses of LM_{ORI}+CM_{ORI} neurons (Fig. 6A) suggested that these neurons responded strongly to LM gratings at 2 and 4 cpd, with preferred SFs around 1–2 cpd. However, they barely responded to CM gratings at 2–8 cpd, even if 2 cpd was near their mean preferred SFs with LM stimuli. As a result, these neurons preferred approximately 1 cpd with CM gratings. This trend was confirmed by the difference in frequency distributions of preferred SFs between LM and CM neurons (all SF tuned neurons with current LM and CM stimuli, respectively) (Fig. 6B). The median preferred SF was 2.35 cpd with LM neurons and 0.91 cpd with CM neurons. These results provided direct evidence that our CM data were little affected by screen luminance nonlinearity.

4. Discussion

Our results demonstrate that many V1 superficial-layer neurons are orientation-selective with both LM and CM stimuli, which is in agreement with previous studies that at least part of the A17/V1 neurons respond to both LM and CM stimuli (Zhou and Baker, 1994; El-Shamayleh and Movshon, 2011; An et al., 2014; G. Li et al., 2014). A certain percentage of neurons (10–20%) are tuned to CM orientation only, which would have reduced the chance of finding orientation-selective CM neurons in previous single-unit studies because RF mapping is typically performed with LM stimuli.

Evidence from orientation adaptation experiments may shed light on the mechanisms underlying neuronal LM and CM responses. As Figs. 4 & 5 indicate, neurons' peak LM and CM responses are similarly (Fig. 4) or nearly similarly (Fig. 5) suppressed by LM and CM adaptors, indicating possibly shared neural mechanisms underlying LM and CM processing. Moreover, orthogonal orientation adaptation, although weaker than iso-orientation adaptation, is quite robust, which may suggest a sizeable orientation unspecific component in neuronal responses to LM and CM stimuli. Previous studies tended to find less orthogonal orientation adaptation (see a review by Kohn, 2007) than what we found. In our study, many neurons' responses at orthogonal orientations are above zero ($\Delta F/F > 0$, Figs. 2B, 4B, & 5B). Our previous two-photon imaging studies have shown that the same V1 neurons showing above-zero responses to orthogonal orientations (Ju et al., 2021) become non-responsive ($\Delta F/F = 0$) at non-preferred SFs (Guan et al., 2021), suggesting that these orthogonal orientation responses are not artifacts of two-photon calcium imaging or specific stimulus conditions (e.g., high contrast). Rather, they are consistent with reports that many V1 cells show higher-than-spontaneous-level responses at orthogonal orientations (Knierim and van Essen, 1992; Ringach et al., 2002), which suggests an orientation unspecific component in V1 orientation responses. As a result, orthogonal orientation adaptation is expected to reduce neuronal responses at all orientations, including the preferred orientation, as shown in Figs. 4 and 5.

Our results are reminiscent of the classical view that V1 simple cell receptive fields pool outputs from aligned ON- or OFF-center LGN cell receptive fields (Hubel and Wiesel, 1962; K. Tanaka, 1985; Reid and Alonso, 1995). Here simple cells' pooling of the same-sign LGN inputs suggests summation of half-wave rectified outputs of LGN cells, which is essentially a filter-rectify-filter process. Because LGN neurons have little orientation preferences, LM adaptors and the bright and dark elements of CM adaptors regardless of orientation can at least partially suppress the responses of aligned ON- and OFF-center LGN neurons (Solomon et al., 2004; Camp et al., 2009). For example, Camp et al. (2009) reported that the gains of parvocellular LGN cells are reduced by 37.5% after adaptation, which is in the range of the orthogonal LM-LM adaptation effects (Fig. 4D) with V1 superficial-layer neurons that receive predominant excitatory drive from the parvocellular input layer (4Cβ). These orientation-unspecific adaptation effects would then be inherited by downstream V1 neurons (Dhruv and Carandini, 2014). Additional roles of recurrent intracortical excitation and inhibition have been proposed to sharpen the orientation tuning of V1 neurons (Ben-Yishai et al., 1995; Douglas et al., 1995; Somers et al., 1995). For LM stimuli, these intracortical influences appear to have weak effects with the current high contrast stimuli, as the adaptation effects at the iso and orthogonal orientations were only moderately different. However, the proposed intracortical interactions (Ben-Yishai et al., 1995; Douglas et al., 1995; Somers et al., 1995) may sharpen CM neurons' orientation tuning more substantially. Accordingly, adaptation at CM neurons' preferred orientations suppresses orientation-unspecific subcortical contributions to CM responses, as well as orientation-specific intracortical contributions, producing much higher iso adaptation effects than orthogonal adaptation effects (Fig. 5). This ad hoc analysis does not require special mechanisms for CM processing in V1, but only involves known mechanisms of subcortical response pooling and intracortical interactions. The analysis is also similar to the original FRF model on texture perception by Bergen and Adelson (1988), in that subcortical and V1 neurons serve as the first- and second-stage linear filters, respectively.

Because of the limitations of current two-photon calcium technology, we are only able to record the responses of neurons in very superficial V1 layers (150–300 μm below the cortical surface). Therefore, we cannot exclude V1 layer 4 C neurons, which receive direct thalamic inputs (K. Tanaka, 1985; Reid and Alonso, 1995), serving as initial orientation nonspecific filters for CM processing. Moreover, one reviewer pointed out that orientation unspecific CM responses may come from neighboring non-orientation tuned neurons. These neurons accounted for about 10% of total identified neurons in Monkeys A-D, much less than CM neurons that accounted for 45–55% (or 40–50% of orientation-tuned neurons, Fig. 3A), and little is presently known regarding the interactions between orientation-tuned and untuned neurons in V1 superficial layers. Nevertheless, it is possible that these neighboring neurons may contribute, but not fully, to orientation-nonspecific CM responses. On the other hand, because of the slowness of calcium signals, we cannot identify the possible roles of feedback in V1 neurons' responses to CM stimuli. Additional causal studies with different technologies will help further probe the circuit mechanisms underlying CM processing, which include subcortical and

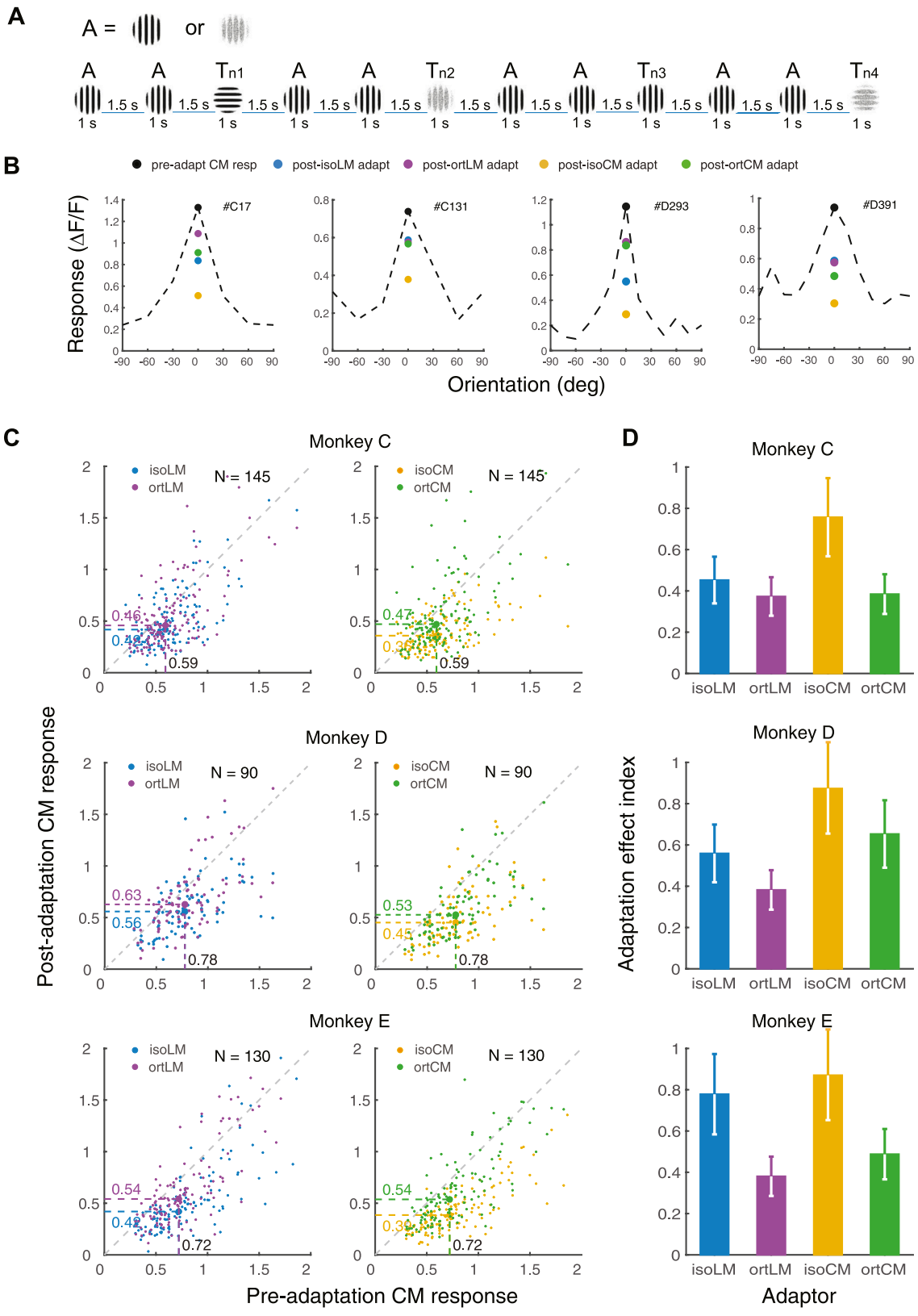

Fig. 5. The effects of adaptation on V1 responses to CM gratings. A. Another illustration of an adaptation stimulus sequence $AAT_{n1}AAT_{n2}AAT_{n3}AAT_{n4}$. A was a LM (shown in the sequence) or CM adaptor at one of six orientations. $T_{n1\text{-}n4}$ were the LM and CM gratings whose orientations were either the same as, or orthogonal to, the adaptor orientation, and were presented in a random order. B. The orientation tuning function of four example neurons with CM gratings and the responses at the peak orientation after adaptation to four types of adaptors. C. Scatterplots of individual neurons' CM responses at the peak orientation before and after adaptation to 4 types of adaptors. The dashed lines indicate median responses. Left panels: Results with LM adaptors. Right panels: Results with CM adaptors. D. The adaptation effect indices for CM responses with 4 types of adaptors. Similar results were obtained when AEI data with CM_{ORI_only} neurons and LM_{ORI}+CM_{ORI} neurons were analyzed separately (Fig. S3B). Error bars show 25 and 75 percentiles.

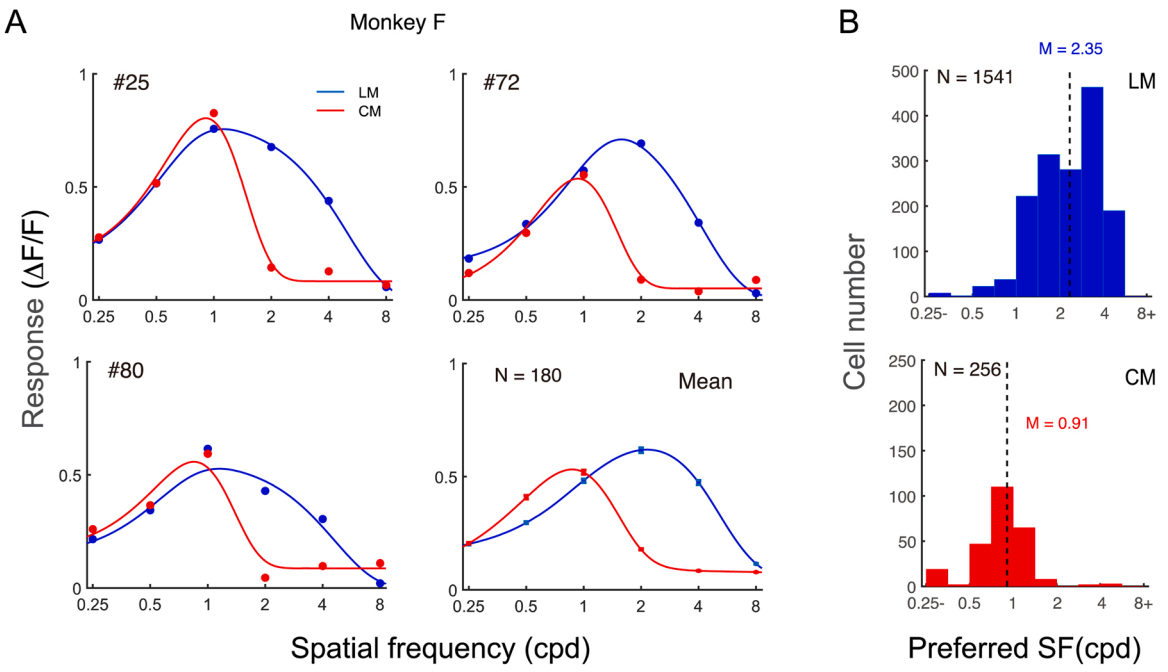

Fig. 6. The effects of potential monitor nonlinearity on CM responses. A. Three example SF tuning functions and the mean SF tuning functions of LM_{ORI}+CM_{ORI} neurons with LM and CM stimuli. The noise elements of CM stimuli were mostly invisible at 2, 4, and 8 cpd. The SF tuning functions were fitted with a Difference-of-Gaussian model. B. Frequency distributions of LM (upper) and CM (lower) neurons at various preferred SFs. The vertical dashed lines indicate median preferred SFs.

intra-cortical mechanisms, as well as feedback mechanisms from downstream visual areas.

The CM stimuli we use are binary noise multiplied by a Gabor function (Fig. 2A), similar to those in several psychophysical and brain imaging studies (Nishida et al., 1997; Larsson et al., 2006; Ashida et al., 2007; An et al., 2014). They are different from contrast envelopes commonly used in neuronal recording studies, which are made by multiplication of a low-SF grating (as the envelope) and a high-SF grating (as the carrier) of different orientations (Zhou and Baker, 1994; El-Shamayleh and Movshon, 2011; G. Li et al., 2014; Gharat and Baker, 2017). One concern with contrast envelope stimuli is that two overlapping gratings at different orientations are expected to elicit cross-orientation suppression, which occurs even when the gratings differ greatly in spatial frequency (Morrone et al., 1982; Bonds, 1989; DeAngelis et al., 1992). Such suppression might be to some degree responsible for the weak V1 evidence for contrast envelope processing in single-unit studies (Zhou and Baker, 1994; El-Shamayleh and Movshon, 2011). As our recent two-photon imaging evidence suggests, some V1 neurons actually prefer plaid stimuli (formed by two intersecting gratings) to Gabor gratings (Guan et al., 2020). However, these plaid neurons are likely excluded during initial receptive field mapping in single-unit recording studies because plaid neurons tend not to respond much to gratings. One missing link is whether V2 or A18, where more CM neurons have been discovered with contrast envelope stimuli (Zhou and Baker, 1994; El-Shamayleh and Movshon, 2011; G. Li et al., 2014), contain substantially more plaid neurons.

Finally, our adaptation evidence, which suggests more upstream FRF processing from subcortical to V1 (see earlier discussion), is different from psychophysical (Nishida et al., 1997) and fMRI adaptation results (Nishida et al., 1997; Larsson et al., 2006; Ashida et al., 2007) that show little cross adaptation effects between LM and CM stimuli. Assuming these early studies had not been affected by the small number of participants (e.g., total N = 14 in three cited fMRI studies), the results are at odds with the FRF models in general by suggesting independent LM and CM processing. Some fMRI evidence indicates that CM processing involved higher brain areas such as V3, V4, and MT+ (Larsson et al., 2006; Ashida et al., 2007). It is possible that psychophysical and fMRI adaptation results are also affected by later and more cognitive stages of CM processing. For example, high brain areas may process LM and CM stimuli independently on the basis of their appearance differences.

Acknowledgments

This study was supported by Ministry of Science and Technology, China grant 2022ZD0204601, Natural Science Foundation of China grants 31230030 and 31730109, and funds from Peking-Tsinghua Center for Life Sciences, Peking University. We thank comments and suggestions from Curtis Baker, Michael Landy, Hai-Dong Lu, and Wei Wang during the preparation of this manuscript.

Appendix A. Supporting information

Supplementary data associated with this article can be found in the online version at doi:10.1016/j.pneurobio.2022.102315.

References

An, X., Gong, H., Yin, J., Wang, X., Pan, Y., Zhang, X., Lu, Y., Yang, Y., Toth, Z., Schiessl, I., McLoughlin, N., Wang, W., 2014. Orientation-cue invariant population responses to contrast-modulated and phase-reversed contour stimuli in macaque V1 and V2. PLoS One 9, e106753.

Ashida, H., Lingnau, A., Wall, M.B., Smith, A.T., 2007. FMRI adaptation reveals separate mechanisms for first-order and second-order motion. J. Neurophysiol. 97, 1319–1325.

Ben-Yishai, R., Bar-Or, R.L., Sompolinsky, H., 1995. Theory of orientation tuning in visual cortex. Proc. Natl. Acad. Sci. USA 92, 3844–3848.

Bergen, J.R., Adelson, E.H., 1988. Early vision and texture perception. Nature 333, 363–364.

Bergen, J.R., Landy, M.S., 1991. Computational modeling of visual texture segregation. In: Landy, M.S., Movshon, J.A. (Eds.), Computational models of visual form, shape, and object recognition processing. MIT Press, Cambridge, MA, pp. 253–271.

Bonds, A.B., 1989. Role of inhibition in the specification of orientation selectivity of cells in the cat striate cortex. Vis. Neurosci. 2, 41–55.

Camp, A.J., Tailby, C., Solomon, S.G., 2009. Adaptable mechanisms that regulate the contrast response of neurons in the primate lateral geniculate nucleus. J. Neurosci. 29, 5009–5021.

Carandini, M., Heeger, D.J., Movshon, J.A., 1999. Linearity and gain control in V1 simple cells. In: Jones, E.G., Ulinski, P.S. (Eds.), Cerebral Cortex, vol. 13. Cortical Models. Kluwer Academic/Plenum, New York, pp. 401–443.

DeAngelis, G.C., Robson, J.G., Ohzawa, I., Freeman, R.D., 1992. Organization of suppression in receptive fields of neurons in cat visual cortex. J. Neurophysiol. 68, 144–163.
Demb, J.B., Zaghloul, K., Sterling, P., 2001. Cellular basis for the response to second-order motion cues in Y retinal ganglion cells. Neuron 32, 711–721.
Dhruv, N.T., Carandini, M., 2014. Cascaded effects of spatial adaptation in the early visual system. Neuron 81, 529–535.
Douglas, R.J., Koch, C., Mahowald, M., Martin, K.A., Suarez, H.H., 1995. Recurrent excitation in neocortical circuits. Science 269, 981–985.
El-Shamayleh, Y., Movshon, J.A., 2011. Neuronal responses to texture-defined form in macaque visual area V2. J. Neurosci. 31, 8543–8555.
Fechner, G.T., 1860. Elemente der Psychophysik. Leipzig: Breitkopf und Hertel. In: Adler, H.E. (Ed.), Elements of Psychophysics. Holt, Rinehart, and Winston, New York.
Ferster, D., Chung, S., Wheat, H., 1996. Orientation selectivity of thalamic input to simple cells of cat visual cortex. Nature 380, 249–252.
Gharat, A., Baker Jr., C.L., 2017. Nonlinear Y-like receptive fields in the early visual cortex: an intermediate stage for building cue-invariant receptive fields from subcortical Y cells. J. Neurosci. 37, 998–1013.
Graham, N., 1989. Visual Pattern Analyzers (Oxford Psychology Series, No. 16). Oxford University Press, New York.
Graham, N., Sutter, A., 1998. Spatial summation in simple (Fourier) and complex (non-Fourier) texture channels. Vis. Res. 38, 231–257.
Guan, S.C., Zhang, S.H., Zhang, Y.C., Tang, S., Yu, C., 2020. Plaid detectors in macaque V1 revealed by two-photon calcium imaging. Curr. Biol. 30, 934–940.
Guan, S.C., Ju, N., Tao, L., Tang, S.M., Yu, C., 2021. Functional organization of spatial frequency tuning in macaque V1 revealed with two-photon calcium imaging. Prog. Neurobiol. 205, 102120.
Hallum, L.E., Movshon, J.A., 2014. Surround suppression supports second-order feature encoding by macaque V1 and V2 neurons. Vis. Res. 104, 24–35.
Hubel, D.H., Wiesel, T.N., 1959. Receptive fields of single neurones in the cat's striate cortex. J. Physiol. 148, 574–591.
Hubel, D.H., Wiesel, T.N., 1962. Receptive fields, binocular interaction and functional architecture in the cat's visual cortex. J. Physiol. 160, 106–154.
Ju, N., Guan, S.C., Tao, L., Tang, S.M., Yu, C., 2021. Orientation tuning and end-stopping in macaque V1 studied with two-photon calcium imaging. Cereb. Cortex 31, 2085–2097.
Knierim, J.J., van Essen, D.C., 1992. Neuronal responses to static texture patterns in area V1 of the alert macaque monkey. J. Neurophysiol. 67, 961–980.
Kohn, A., 2007. Visual adaptation: physiology, mechanisms, and functional benefits. J. Neurophysiol. 97, 3155–3164.
Landy, M.S., Oruc, I., 2002. Properties of second-order spatial frequency channels. Vis. Res. 42, 2311–2329.
Larsson, J., Landy, M.S., Heeger, D.J., 2006. Orientation-selective adaptation to first- and second-order patterns in human visual cortex. J. Neurophysiol. 95, 862–881.
Li, G., Yao, Z., Wang, Z., Yuan, N., Talebi, V., Tan, J., Wang, Y., Zhou, Y., Baker Jr., C.L., 2014. Form-cue invariant second-order neuronal responses to contrast modulation in primate area V2. J. Neurosci. 34, 12081–12092.
Li, M., Liu, F., Jiang, H., Lee, T.S., Tang, S., 2017. Long-term two-photon imaging in awake macaque monkey. Neuron 93, 1049–1057 e1043.
Morrone, M.C., Burr, D.C., Maffei, L., 1982. Functional implications of cross-orientation inhibition of cortical visual cells. I. Neurophysiological evidence. Proc. R. Soc. Lond. B Biol. Sci. 216, 335–354.
Nishida, S., Ledgeway, T., Edwards, M., 1997. Dual multiple-scale processing for motion in the human visual system. Vis. Res. 37, 2685–2698.
Pelli, D.G., Zhang, L., 1991. Accurate control of contrast on microcomputer displays. Vis. Res. 31, 1337–1350.
Reid, R.C., Alonso, J.M., 1995. Specificity of monosynaptic connections from thalamus to visual cortex. Nature 378, 281–284.
Ringach, D.L., Shapley, R.M., Hawken, M.J., 2002. Orientation selectivity in macaque V1: diversity and laminar dependence. J. Neurosci. 22, 5639–5651.
Rosenberg, A., Husson, T.R., Issa, N.P., 2010. Subcortical representation of non-Fourier image features. J. Neurosci. 30, 1985–1993.
Solomon, S.G., Peirce, J.W., Dhruv, N.T., Lennie, P., 2004. Profound contrast adaptation early in the visual pathway. Neuron 42, 155–162.
Somers, D.C., Nelson, S.B., Sur, M., 1995. An emergent model of orientation selectivity in cat visual cortical simple cells. J. Neurosci. 15, 5448–5465.
Tanaka, H., Ohzawa, I., 2009. Surround suppression of V1 neurons mediates orientation-based representation of high-order visual features. J. Neurophysiol. 101, 1444–1462.
Tanaka, K., 1985. Organization of geniculate inputs to visual cortical cells in the cat. Vis. Res. 25, 357–364.
Zhou, Y.X., Baker Jr., C.L., 1994. Envelope-responsive neurons in areas 17 and 18 of cat. J. Neurophysiol. 72, 2134–2150.